

Designing a NISQ reservoir with maximal memory capacity for volatility forecasting

Samudra Dasgupta
Bredesen Center,
University of Tennessee,
Knoxville, Tennessee, USA
sdasgup3@vols.utk.edu

Kathleen Hamilton
Quantum Computational Science,
Oak Ridge National Laboratory
Oak Ridge, Tennessee, USA
hamiltonke@ornl.gov

Arnab Banerjee
Department of Physics,
Purdue University
West Lafayette, Indiana, USA
arnabb@purdue.edu

Abstract—Current noisy intermediate-scale quantum (NISQ) devices are far from being fault-tolerant, however, they permit some limited applications. In this study, we use a hybrid quantum-classical reservoir computing model to forecast the CBOE volatility index (VIX) using the S&P500 (SPX) time-series. The NISQ component of our model is executed on IBM’s 53 qubit Rochester chip. We encode the SPX values in the rotation angles and linearly combine the average spin of the six-qubit register to predict the value of VIX at next time step. Our results demonstrate a potential approach towards utilizing noisy quantum devices for non-linear time-series forecasting tasks.

I. INTRODUCTION

Accurate forecasting of financial data is a difficult task: financial data is massive and contains many correlated dimensions. Risk estimation needs to strike a balance between avoiding catastrophic crises and avoiding risk altogether. Risk (in finance) is typically measured in terms of volatility of returns or close analogues like Value at Risk [1]. Risk can be unconditional, for example the 30-day rolling standard deviation of the S&P 500 Index (SPX) returns. It can also be conditional, for example Expected Shortfall which is defined as the average loss given the loss has crossed a certain threshold. The observed price of options in the markets can help impute the implied volatility. Developing useful machine learning based models for financial forecasting tasks requires memory characteristics that balance long-term and short-term risk.

The field of reservoir computing (RC) [2] provides a detailed but flexible road map towards using signal-driven dynamical systems to process information with non-von Neumann architectures. RC models are useful in providing alternatives to deep learning that can deliver comparable performance yet are low energy, and computationally simple. They are capable of both one-shot and continuous real-time learning and excel at non-linear function approximation tasks. RC systems have been utilized in many different applications and can be constructed from many different dynamical systems (see recent reviews [3], [4]).

Quantum reservoir computing (QRC) uses quantum ensembles for information processing. In a recent work [5], quantum spin systems were used to construct a quantum reservoir and used for predicting non-linear time series. Reservoirs built using superconducting qubits are demonstrated in [6], [7] and these studies have developed a theoretical underpinning behind

the ability to use dissipative quantum systems as quantum counterpart to approximating non-linear input-output maps using classical dynamical systems.

A. Related Works

Understanding the computational capacity of quantum reservoirs is an open question. There have been several approaches to quantum reservoir designs and numerical experiments show that quantum systems consisting of 5–7 qubits possess computational capabilities comparable to conventional recurrent neural networks of 100 to 500 nodes [8]. Additionally, small quantum systems also demonstrate significant computational capacities [9]. A recent study [10] has also focused on optimizing quantum reservoirs for time series forecasting for financial data (the S&P 500 index). Our study is comparable to [6] and [7] but differ in the following way;

- We are focused on hybrid quantum-classical reservoirs (which we refer to as NISQ reservoirs) which incorporate quantum circuits and classical feedback elements.
- We implement systematic design considerations of these NISQ reservoirs as a computing engine which should be useful for practitioners.
- We address the question of evaluating the memory capacity of various reservoir topologies and how to select the optimal one.
- We handle the case of a ‘real-life signal’ that cannot be expressed by an analytical deterministic equation. VIX (see Section IV-A) is intrinsically related to market fluctuations and trader psychology.

B. Organization and contribution

In this study, we focus on the task of VIX forecasting, using the SPX return as the independent variable. Given that ΔSPX explains less than 75% of ΔVIX , we acknowledge that sophisticated implementations would use more economic indicators (such as the unemployment rate, gross domestic product and federal funds rate). However, the focus of this study is demonstrating the design and use of a NISQ reservoir for forecasting purposes and not pushing the envelope on forecasting accuracy.

We provide a high-level overview of reservoir computing in II. We characterize the memory capacity of a six-qubit NISQ

reservoir in Section III. This characterization determines the reservoir design used in Section IV to forecast the VIX index. In Section IV, we discuss the relevant properties of the VIX index, the input encoding methodology, the NISQ reservoir circuit construction, the use of post-processing and feedback and finally the results of the forecasting task. Section V concludes with a summary of the contributions of this study.

II. OVERVIEW OF RESERVOIR COMPUTING

Classical reservoir computing (RC) relies on a reservoir of randomly connected oscillators. The connections between the oscillators in the reservoir are not trained. In this computational framework, inputs are mapped to a high dimensional space and the output from the high dimensional state is trained to predict the desired function using a simple method like linear regression. RC using a simple readout is suited to low-cost real-time computing history dependent dynamical responses to external inputs. Let $\mathbf{x}(n)$ denote the reservoir state vector:

$$\mathbf{x}(n) = \begin{bmatrix} x_0(n) \\ x_1(n) \\ \vdots \\ x_{N-1}(n) \end{bmatrix} \quad (1)$$

Here each x_i represents the state of a node in the reservoir. This state vector undergoes a non-linear evolution in time.

Quantum Reservoir Computing (QRC) is a new, alternative paradigm for information processing using quantum physics. It exploits natural quantum dynamics of ensemble systems for machine learning. The key is to find an appropriate form of physics that exhibits rich dynamics, thereby allowing us to outsource a part of the computation. There have been several applications of QRC most notably time-dependent signal processing, speech recognition, NLP, sequential motor control of robots, and stock market predictions. QRC does not require any sophisticated quantum gate (natural dynamics is enough). Thus it exhibits high feasibility. Numerical experiments show that quantum systems consisting of 5–7 qubits possess computational capabilities comparable to conventional recurrent neural networks of 100 to 500 nodes [8].

Unlike traditional neural networks, we do not currently understand the guiding principles for designing non-von-Neumann architectures (such as the brain-inspired reservoir computers for high-performance information processing). Below, we give a brief overview of some of the important considerations:

- 1) Common Signal Induced Synchronization: If the reservoir has two different initial state $s(t_0)$ and $\hat{s}(t_0)$, then, if provided with the same input stimuli $\{u(t)\}_{t \geq t_0}$, it must satisfy,

$$\|s(t) - \hat{s}(t)\| \rightarrow 0 \text{ as } t \rightarrow \infty. \quad (2)$$

Another way of stating this is that the reservoir must have fading memory (also known as echo state property in literature): the outputs of the dynamical system should stay close if the corresponding input are close in recent times [11]. This can be viewed as a consistency or convergence

criterion, it ensures that any computation performed by the reservoir is independent of its initial condition.

- 2) Reservoir Dimensionality: A reservoir should have adequate (preferably exponential in number of nodes) linearly independent internal variables. The number of linearly independent variables of the NISQ reservoir (the Hilbert space dimension) gives an upper limit on the computational capacity. As noted in [12] prediction accuracy improves as you increase the number of nodes in the system.
- 3) Adequate Memory: A reservoir can have memory of past inputs [13]. Using a one qubit reservoir for simplicity, let's understand how memory manifests in a dynamical system. Suppose $u(t)$ and $\hat{u}(t)$ are two identical time series, except for a small perturbation at $t = t_0 - 1$:

$$\begin{aligned} \hat{u}(t_0 - 1) &= u(t_0 - 1) + \Delta, \text{ for } t = t_0 - 1, \\ \hat{u}(t) &= u(t), \text{ for all } t \neq t_0 - 1. \end{aligned}$$

When we feed $u(t)$ or $\hat{u}(t)$ into the quantum circuit, we get the spin (measured along the Z direction) time series $\{s(t)\}$ and $\{\hat{s}(t)\}$ respectively. If $\delta s(t) = s(t) - \hat{s}(t)$ denotes the difference between the outputs $s(t)$ and $\hat{s}(t)$, then we say the reservoir has memory when $\delta s(t)$ and $\delta s(0)$ are related (i.e. $\delta s(t)$ can provide information about $\delta s(0)$). Higher mutual information between $\delta s(t)$ and $\delta s(0)$ implies higher MC. A formal proof is given in [11]. A linear circuit has higher MC as $\delta s(t)$ is strongly correlated with $\delta s(0)$. Thus high degree of linearity is more suitable for forecasting tasks which need to recall historical patterns. This implies that to introduce linear elements in the NISQ reservoir we will need to introduce 'self-loops' in the spin-system.

- 4) Response Separability: The separation property is the reservoir's capability to generate dynamics sufficiently rich that can distinguish between any two different input sequences. This is important because it is not enough that the reservoir is excitable by the input sequence you care about. It should be excitable by any distinguishable inputs and the (input history dependent) response should be adequately distinguishable [14].
- 5) Adequate Non-linearity: Non-linearity is required for effective functioning of reservoir computers to address the 'linearly inseparable problem' [15] A non-linear transformation is mandatory for tasks such as classification by support vector machines. This property turns out to be crucial for achieving universal computing. However, non-linearity also degrades memory. Thus a careful trade-off is required between the linear and non-linear elements of the circuit.
- 6) Edge Density: Edge density is a system level metric (as opposed to node level metric) that is an important driver of the predictive power achieved by a hybrid reservoir. We quantitatively define edge density as the ratio of the total number of edges present in the reservoir configuration to the total number of possible edges. A discussion on how heightened non-linearity in the system due to increased

connectivity leads to MC degradation can be found in [11].

- 7) **Feedback Strength:** To be an effective forecasting engine, the reservoir has to strike a balance between two competing aims: memorizing past patterns (which is related to over-fit reduction) and reducing mean square error (which is related to fit accuracy). The former requirement asks for the ‘state signal’ to play a dominant role (as the reservoir memorizes through the time evolution of its quantum spin state) while the latter pushes the ‘incoming signal pattern’ to have more weighting. This tunable parameter can be used in the system evolution specification.
- 8) **Noise induced regularization:** The use of dissipative quantum systems as universal function approximators for temporal information processing, especially in the presence of noisy data, is well known. Indeed, noise can be beneficial in machine learning related information processing tasks where it plays a role akin to regularization [16], i.e., makes the solution space more acceptable and realistic. Training on noisy data avoids over-fitting which helps NISQ reservoirs avoid converging to extreme, unrealistic values in forecasting related tasks.

III. MEMORY CAPACITY

Memory capacity (MC) quantifies the ability of the reservoir to forecast at different time-scales. Before we can design our reservoir, we characterize the MC of different possible configurations of the reservoir, following the approach given in [5]. The configuration with the highest MC is then used for the time-series prediction task in Section IV.

Let u_k be the time-series one is trying to forecast (where k denotes the time index). Let $\hat{u}_{k-\tau}$ denote the forecast of \hat{u}_k using information till time-step $k - \tau$. The correlation r_τ between $\hat{u}_{k-\tau}$ and u_k is a measure of how well the system is able to do a τ step look-ahead prediction:

$$r_\tau^2 = \frac{\text{COV}(u_{k-\tau}, \hat{u}_{k-\tau})}{\sigma^2(u_{k-\tau})\sigma^2(\hat{u}_{k-\tau})}, \quad (3)$$

where $\text{COV}(x, y)$ denotes the covariance between x and y and $\sigma(x)$ denotes the standard deviation of x . Intuitively, one expects that the larger the value of τ , the lower is the value of r_τ (as higher the value of τ , more amount of recent data is ignored).

The MC is the sum of r_τ^2 over different values of τ :

$$MC = \sum_{\tau=1}^{\tau_{max}} r_\tau^2. \quad (4)$$

As in [5], we use a random sequence $\in [0, 1]$ for u_k (where k denotes the time index) and fix the maximum value of τ to be $\tau_{max} = 120$. This is done to ensure that the MC benchmark does not depend on a specific time-lag or a specific signal structure.

The NISQ reservoirs used in this study are hybrid quantum-classical systems. The demarcation between classical and quantum resources is shown in Fig. 1. The first classical layer transforms the input into a qubit angle encoding. The quantum

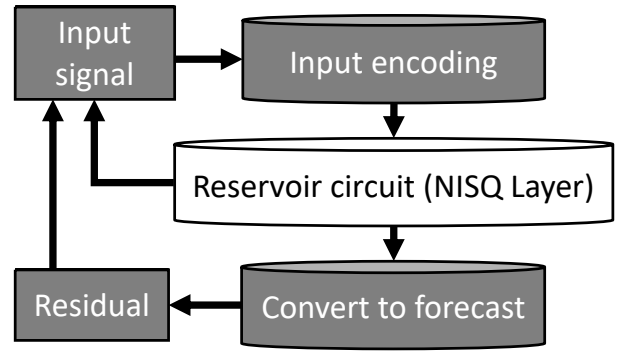


Fig. 1. Schematic of the hybrid quantum-classical reservoir (NISQ reservoir) system which consists of classical inputs and outputs (grey boxes), classical computational layers (grey cylinders) and quantum computational layers (white cylinder).

layer is used to generate an array of N -qubit spin values. The final classical layer is used to compute the forecast, and the forecast error. Both the forecast error and spin values are fed back into the first classical layer.

We characterize the MC of a 6-qubit NISQ reservoir as a function of recurrent connections using a sequence of $1 + N + N(N-1)/2$ graphs in increasing order of network connectivity (and hence complexity). The first term in the sequence is an empty graph on N vertices. The next N terms in the sequence are sequentially constructed by adding self-loops to each vertex. The next N terms are sequentially constructed by connecting the N vertices into a simple cycle. Finally the remaining $(N(N-1)/2)$ terms of the sequence are constructed by sequentially connecting vertices until the final circuit is a fully connected graph with N self-loops. Note that an edge can be realized between any two nodes of the reservoir if a two-qubit gate is placed between the qubits in the quantum layer; or if the output of one qubit is fed to another qubit during the classical pre-processing layer. For a 6 qubit system, 22 configurations are possible. This sequence is shown in Fig. 2.

The MC of each reservoir was evaluated using IBM’s 53 superconducting qubit platform (`ibmq_rochester`) and is shown in Fig. 3. A peak in the MC (within the bounds of statistical significance of the MC) is observed for reservoirs with 5 self-loops. This reservoir design is then chosen for the information processing in Section IV.

There are three underlying drivers for this observed peak:

- 1) Linear nodes increase memory capacity. Linear nodes are nodes with linear activation function such as

$$\phi(s_{t+1}) = as_t + b \quad (5)$$

Here, s refers to average spin of the quantum register. Self-loops, by definition, are the configurations where the output of quantum register element m at time t is utilized to calculate the angle for the rotation gates at time $t + 1$. See [11] for a detailed discussion on how linear elements enhance memory capacity. For configuration sequences 1 to 7, there is a steady increase in number of self-loops but

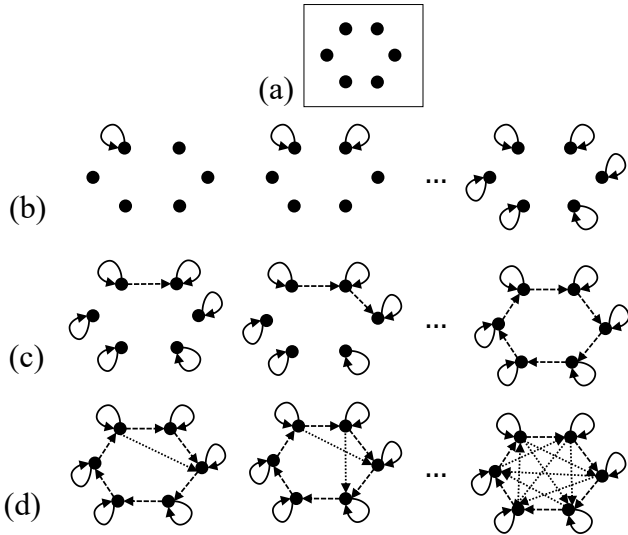


Fig. 2. Sequence of reservoir complexity circuits: (a) The first term is always an empty graph on N qubits, (b) The first (N) circuits are generated by adding self-loops, (c) The next (N) circuits are generated by connecting the qubits into a simple cycle, (d) The remaining circuits are generated by adding edges to fully connect all N qubits.

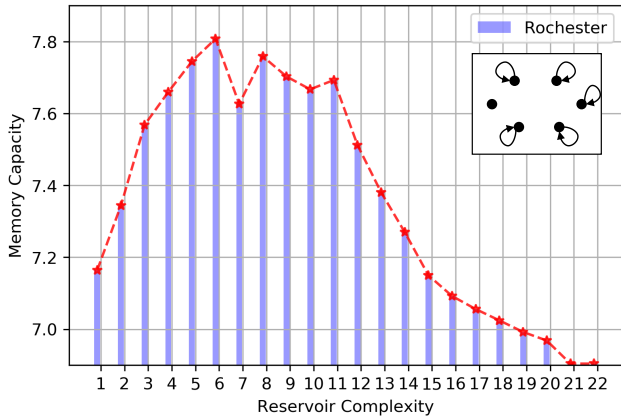


Fig. 3. MC as a function of reservoir complexity for a 6-qubit reservoir executed on `ibmq_rochester`. [Inset] The optimal reservoir topology with self-loops on 5 qubits.

after that the nodal activation functions become non-linear and degrade memory (see Fig. 4).

- 2) Feedback strength increases memory capacity as the reservoir tries to remember the *history* of the incoming signal. A stronger feedback increases memory capacity (see Fig. 5). Note that unlike traditional machine learning approaches which use a predetermined window of data for training, here we use a floating window with data from τ day prior as a look-ahead predictor. We adopt this practice of using the most recent data for prediction as is likely to yield the best forecast and is a common prevalence in VIX forecasting (see for example [16], [17]).
- 3) Densely connected reservoirs degrade memory capacity. Density is related to the degree of intra-qubit connectivity.

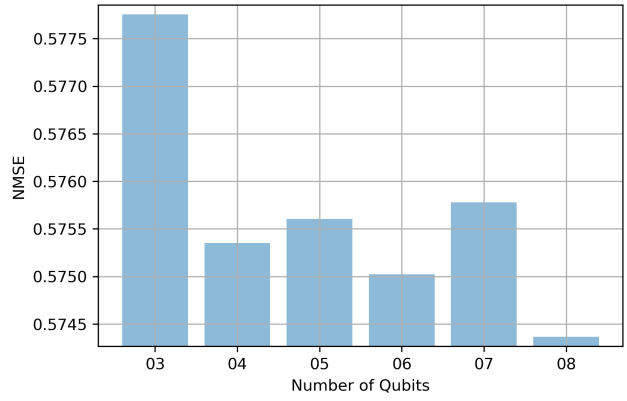


Fig. 4. Dependence between memory capacity and number of self-loops.

Higher relative connection strength increases memory

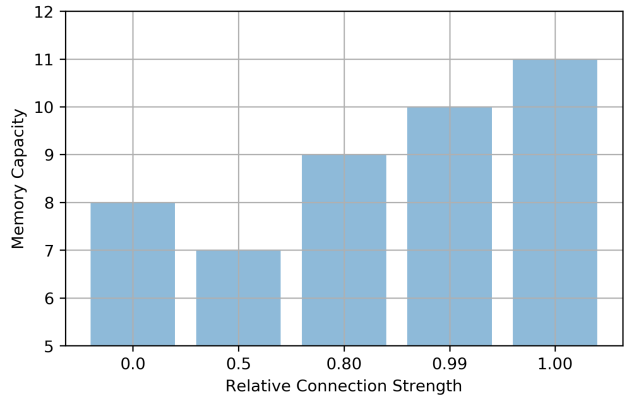


Fig. 5. Dependence between memory capacity and feedback strength

Fig. 6 provides some empirical evidence to show that higher density degrades memory.

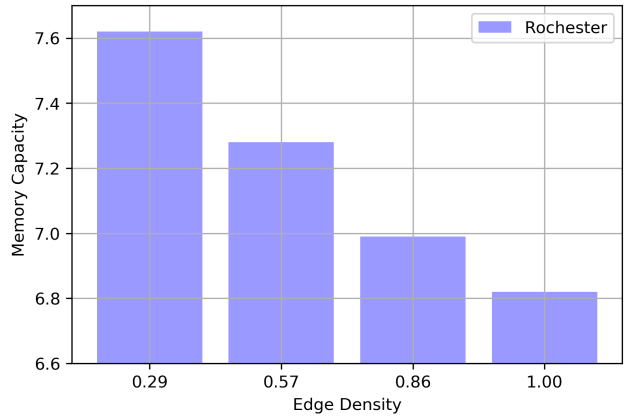


Fig. 6. Dependence between memory capacity and edge density.

The same sequence of reservoir topologies were also simulated in IBM Qiskit [18]. The results of the noiseless simulation are shown in Fig. 7. Comparison with Fig. 3 reveals

that the hardware noisiness translates into higher MC (within the bounds of statistical significance) for circuits with higher connectivity (leading to higher degree of non-linear dynamics). We also observe a slower decay in MC for the NISQ reservoir with hardware noise. This points to a beneficial impact of the noise in today’s NISQ devices.

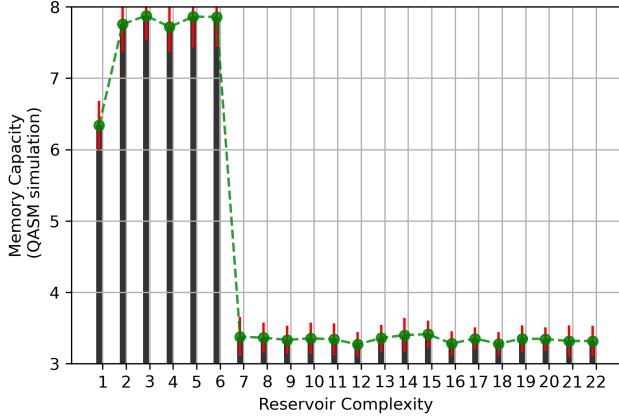


Fig. 7. MC as a function of reservoir complexity for a 6-qubit reservoir simulated with noiseless qubits.

IV. VIX FORECASTING

In the previous section we found the optimal design of the NISQ reservoir (based on maximal MC value). In this section we will first give more background for the economic indicator that we are trying to predict. Then, we will discuss the components of the NISQ reservoir as shown in Fig. 1, tailored to the VIX forecasting task: (a) input encoding (Section IV-B), (b) a quantum circuit (Section IV-C), and (c) forecast and feedback generation (Section IV-D).

In Fig. 8 we show the computational graph associated with this design, tailored for the VIX forecasting task. The input encoding consists of the transformation of $\Delta r(t) \rightarrow u(t)$, the quantum circuit generates the spin values $s_i(t)$ and the forecast is generated by the combination of $s_i(t)$.

A. VIX index forecasting

The VIX index represents the market’s expectation of volatility in the near future as implied by SPX index options data. It is disseminated by CBOE on a real-time basis and modern finance practitioners prefer using VIX for risk estimation. Its value denotes the expected annualized change in the SPX 500 index over the following 30 days, the methodology is detailed in [19]. In short, it is calculated using the CBOE-traded SPX options (which have a non-zero bid-ask) whose expiration falls within next 23 days and 37 days. Using the classical Black Scholes model assumes a time-independent (constant) volatility. However, economists have confirmed that volatility varies with time (hence the name Stochastic Volatility). Stochastic models (like GARCH) significantly improve the prediction accuracy against values observed in the market and are thus valuable

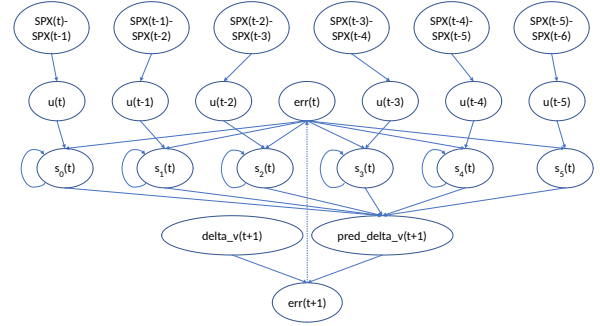


Fig. 8. Computational graph of the 6 qubit reservoir with 5 self-loops: $\Delta r(t) = \text{SPX}(t) - \text{SPX}(t - 1)$, $u(t)$ is the incoming signal post application of a non-linear transformation, $s_i(t)$ is the average spin state of qubit [i], $\text{delta}_v(t+1)$ is the actual value while $\text{pred_delta}_v(t+1)$ is the predicted value. The error residual is denoted by $\text{err}(t+1)$. The residual from time step t is used as feedback to the reservoir.

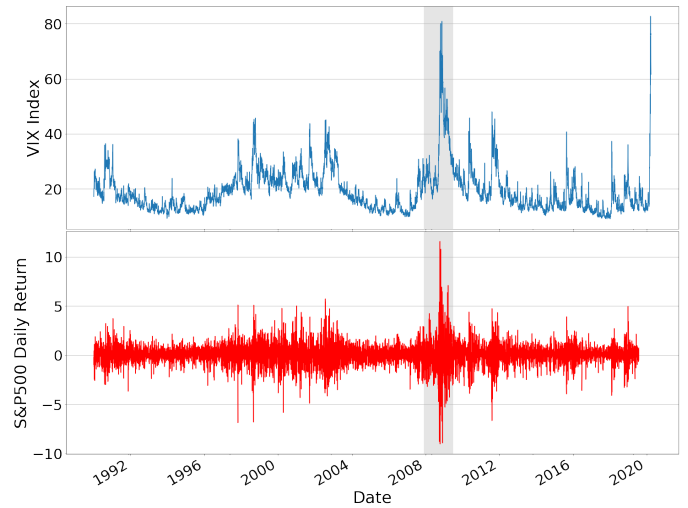


Fig. 9. (Top): The VIX Index plotted as a function of time from January 2, 1990 through March 24, 2020. The data corresponding to the 2008 recession is highlighted in the grey shaded region.(Bottom): The SPX returns ($r(t)$) plotted as a function of time.

in asset pricing (for traders) and asset management (for risk managers).

In this study we develop our NISQ reservoir to forecast the VIX index using the SPX index ($\{r_t\}$) as the independent variable. The entire dataset spans January 2, 1990 through March 24, 2020 (see Fig. 9). The initial one-third of the data (from January 1, 1990 to December 31, 1997) was flushed out to allow the system to stabilize. In Fig. 10 we plot $(\Delta \text{VIX}_t = \text{VIX}_t - \text{VIX}_{t-1})$ versus $(\Delta \text{SPX}_t = \text{SPX}_t - \text{SPX}_{t-1})$.

These are the relevant data properties, as shown in Figs. 9,10:

- VIX is always positive. It is derived from option implied volatility which can never go negative.
- The mean value of the VIX series is approximately 19.



Fig. 10. Scatter plot between the daily percentage change in SPX and daily percentage change in VIX. It should be evident that change in SPX is correlated (negatively) with change in VIX. This is why we use SPX as the main input to the reservoir for VIX forecasting in Section IV-A.

It hit an all time peak of 82.69 on March 16, 2020. The previous maximum value of 80.86 was reached on Nov 20, 2008, at the peak of the mortgage crisis (about eight weeks after the collapse of Lehman Brothers).

- The change in VIX is highly correlated with the change in SPX. The correlation coefficient is approximately -0.74 over the entire date range (though it is much higher during times of crisis). See [20] and [21] for details on why SPX is the primary driver of VIX.
- VIX spikes more when SPX suffers a high negative shock compared to a positive shock of same magnitude. This is referred to as asymmetric volatility in literature and is driven by behavioral psychology.
- VIX exhibits volatility clustering i.e. volatility is persistently high during times of high uncertainty and persistently low during times of more certainty.

B. Input encoding

Let $\{r_t\}$ denote the sequence of time-dependent S&P500 (SPX) log return values [22]:

$$r_t = \log \frac{\text{SPX}_t}{\text{SPX}_{t-1}}. \quad (6)$$

The reservoir predicts a value for VIX at time $(t+1)$ using SPX data for the last seven days $[r(t-6) \cdots r(t)]$. In the classical pre-processing layer, these SPX return values are converted into a vector of rotation angles $\theta(t)$ as follows.

First, the SPX log return values $\{r_t\}$ are differenced:

$$\Delta r_t = r_t - r_{t-1}. \quad (7)$$

Then, a non-linear transformation is applied to $\{\Delta r_t\}$:

$$u(t) = 1 - e^{-(a_0 + a_1 I_t \Delta r_t)}, \quad (8)$$

where I_t is an indicator function

$$I_t = \begin{cases} 1 & \Delta r_t < 0 \\ 0 & \Delta r_t > 0. \end{cases}$$

The non-linear transformation (Eq. 8) is needed to capture the empirical observation (well-known in corporate finance) that when returns go negative, volatility spikes more than when they are positive. This transformation is shown in Fig. 11.

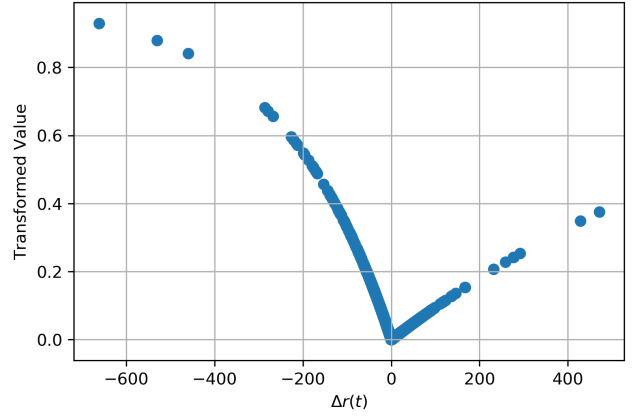


Fig. 11. Transformation applied to Δr to account for volatility asymmetry.

The full encoding of the input signal $(u(t))$ into a vector of rotation values $\theta_m(t)$ uses a heuristic encoding that is dependent on the transformed SPX return $(u(t))$, prediction error e_t , and the average qubit spin $s(t)$ (see following section). The values of $\theta(t)$ are constrained to be in the range $[0, \pi/2]$.

$$\theta_m(t+1) = \begin{cases} \frac{\pi}{2} \left(\alpha u_m(t) + \beta \frac{s_m(t)+1}{2} + \gamma e_t \right) & m \in [0, 4] \\ \frac{\pi}{2} (\alpha' u_m(t) + \gamma' e_t) & m = 5. \end{cases} \quad (9)$$

For the 6-qubit reservoir, the parameters in Eq. 9 are: $\alpha = 0.3, \beta = 0.3, \gamma = 0.4, \alpha' = 0.6, \gamma' = 0.4$.

C. Reservoir circuit

Our NISQ reservoir system consists of a quantum circuit with classical feedback loops. In a classical reservoir the connections between oscillators are not trained, likewise in our NISQ reservoir the connections between qubits are not trained.

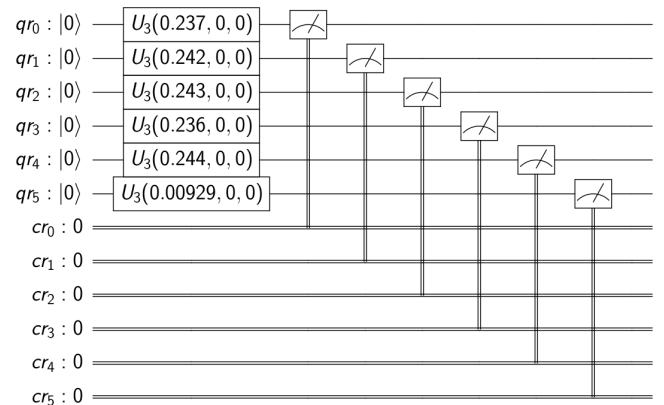


Fig. 12. The 6 qubit quantum circuit executed on `ibmq_rochester` with arbitrary rotation angles. The RY gates are shown as $U3(\theta, \phi = 0, \lambda = 0)$ rotation gates.

The quantum circuit is shown in Fig. 12. It is constructed using only single qubit gates and was executed on `ibmq_rochester`, IBM’s 53 superconducting qubit platform¹. The six qubit register was executed on a subset of hardware qubits selected based on the lowest error rates at the time of job execution. Each circuit was sampled using 8192 shots.

Using the vector of angles found from the classical pre-processing (Section IV-B), the vector element $(\theta(t)[i])$ is passed as the argument to the RY gate on qubit $[i]$. The reservoir does not include any two-qubit gates. When deployed on a NISQ device any interactions between the reservoir nodes are induced by hardware noise (for example: shifts in the implemented angles, cross-talk, and readout noise) and feedback of previous output signals as input.

The output of the reservoir at time t is a vector of average spin values of each qubit $\mathbf{s}(t) = [s_0(t), \dots, s_5(t)]$. Fig. 13 shows the steady state view of the average spin of the 6 qubits in the register.

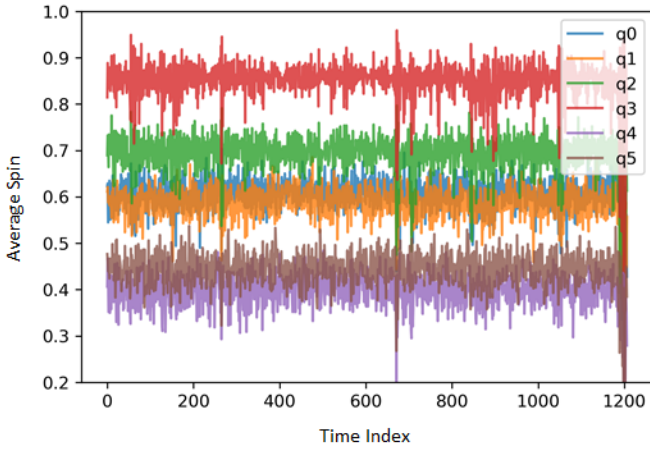


Fig. 13. Steady state view of the average spin of the 6 qubits in the register. These signals are linearly combined by an optimized weight vector to produce the forecast.

D. Post-processing

These six spin values are linearly combined in a classical post-processing layer using a six-dimensional, real-valued weight vector $(\mathbf{w}(t))$ to produce the VIX forecast.

The optimal readout weights are determined by minimizing the mean-square error (MSE) of the VIX value predicted at time (t) . Let σ_{t+1} represent the actual value of the VIX at time t and $\hat{\sigma}_{t+1}$ represent the value predicted by the NISQ reservoir. The residual error is calculated using the MSE:

$$\begin{aligned} \hat{\sigma}_{t+1} &= \mathbf{w}(t) \cdot \mathbf{s}(t), \\ \varepsilon_{t+1} &= \sigma_{t+1} - \hat{\sigma}_{t+1}, \\ \text{MSE} &= \frac{1}{T} \sum_{t=1}^T \varepsilon_t^2. \end{aligned} \quad (10)$$

¹Retired October 31, 2020.

The histogram of residual values (Fig. 14) does not show evidence of any bias.

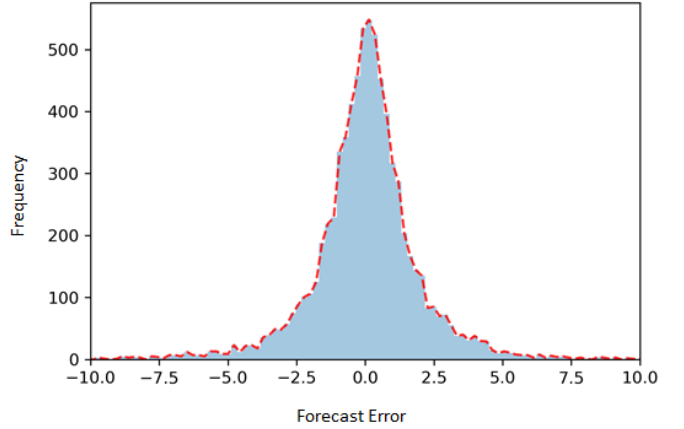


Fig. 14. Forecasting error histogram

The weights are dynamically updated using newly available information. The residual error (the MSE at time-step (t)) is fed back into the reservoir and utilized for determining the rotation angle in next time-step. This provides a negative feedback to minimize the error.

E. Results

In Fig. 16 we plot the one-step ahead forecasts for the 2008 recession. We also plot the change in VIX in Fig. 15 because for effective risk management what matters more is change in volatility.

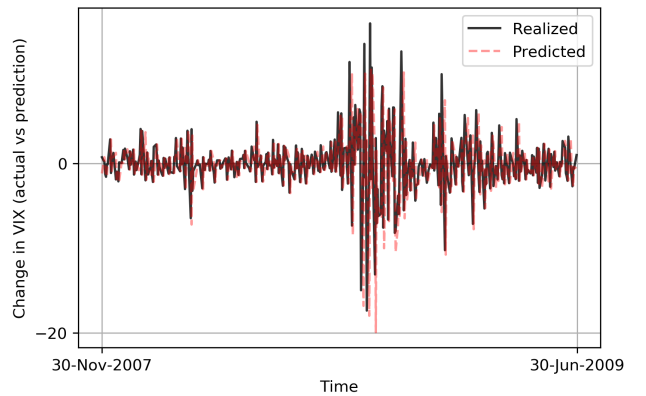


Fig. 15. One step ahead predictions for Δ VIX during the 2008 recession using the NISQ reservoir (red, dashed) compared to the actual values (black, solid).

V. CONCLUSION

NISQ devices are noisy by definition. Examples of noise sources are: qubit decoherence, gate errors and readout error [23], [24]. Such noise can be beneficial in machine learning related information processing tasks akin to regularization [25].

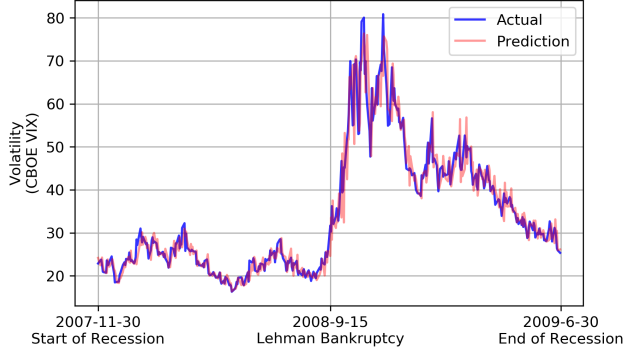


Fig. 16. One step ahead predictions of the VIX index value during the 2008 recession data. Values generated by the quantum reservoir (red) and the actual VIX (blue).

Noise induced regularization helps NISQ reservoirs to be ‘well-behaved’ and avoid taking extreme values in forecasting related tasks.

In this study, we developed a NISQ reservoir for the task of stochastic volatility forecasting in finance - a highly non-linear and memory intensive temporal information processing task which is well-suited for RC [14]. Our results show that that quantum reservoirs implemented with shallow circuits can be used for regression-type analysis in empirical finance and also adaptable for near-term quantum processors.

Promising avenues of future work include analyzing the performance for τ -step look ahead-predictor where $\tau > 1$, tuning the MC of the reservoir to remember historical signal patterns based on a user-defined risk appetite (which will lead to a trade-off with forecast accuracy), evaluating the efficacy of the reservoir in predicting other financial time-series data and accurately modeling the noise dynamics.

ACKNOWLEDGEMENTS

Acknowledgements omitted for double-blind reviewing.

REFERENCES

- [1] A. J. McNeil, R. Frey, and P. Embrechts, *Quantitative risk management: concepts, techniques and tools-revised edition*. Princeton University Press, 2015.
- [2] W. Gerstner, W. M. Kistler, R. Naud, and L. Paninski, *Neuronal dynamics: From single neurons to networks and models of cognition*. Cambridge University Press, 2014.
- [3] J. Dambre, D. Verstraeten, B. Schrauwen, and S. Massar, “Information processing capacity of dynamical systems,” *Scientific reports*, vol. 2, no. 1, pp. 1–7, 2012.
- [4] G. Tanaka, T. Yamane, J. B. Héroux, R. Nakane, N. Kanazawa, S. Takeda, H. Numata, D. Nakano, and A. Hirose, “Recent advances in physical reservoir computing: A review,” *Neural Networks*, vol. 115, pp. 100–123, 2019.
- [5] K. Nakajima, K. Fujii, M. Negoro, K. Mitarai, and M. Kitagawa, “Boosting computational power through spatial multiplexing in quantum reservoir computing,” *Physical Review Applied*, vol. 11, no. 3, p. 034021, 2019.
- [6] J. Chen and H. I. Nurdin, “Learning nonlinear input–output maps with dissipative quantum systems,” *Quantum Information Processing*, vol. 18, no. 7, p. 198, 2019.

- [7] J. Chen, H. I. Nurdin, and N. Yamamoto, “Temporal information processing on noisy quantum computers,” *arXiv preprint arXiv:2001.09498*, 2020.
- [8] K. Fujii and K. Nakajima, “Harnessing disordered-ensemble quantum dynamics for machine learning,” *Physical Review Applied*, vol. 8, no. 2, p. 024030, 2017.
- [9] L. Govia, G. Ribeill, G. Rowlands, H. Krovi, and T. Ohki, “Quantum reservoir computing with a single nonlinear oscillator,” *arXiv preprint arXiv:2004.14965*, 2020.
- [10] A. Kutvonen, K. Fujii, and T. Sagawa, “Optimizing a quantum reservoir computer for time series prediction,” *Scientific reports*, vol. 10, no. 1, pp. 1–7, 2020.
- [11] M. Inubushi and K. Yoshimura, “Reservoir computing beyond memory-nonlinearity trade-off,” *Scientific reports*, vol. 7, no. 1, pp. 1–10, 2017.
- [12] S. Ghosh, A. Opala, M. Matuszewski, T. Paterek, and T. C. Liew, “Quantum reservoir processing,” *npj Quantum Information*, vol. 5, no. 1, pp. 1–6, 2019.
- [13] I. Farkaš, R. Bosák, and P. Gergel’, “Computational analysis of memory capacity in echo state networks,” *Neural Networks*, vol. 83, pp. 109–120, 2016.
- [14] G. Tanaka, T. Yamane, J. B. H  roux, R. Nakane, N. Kanazawa, S. Takeda, H. Numata, D. Nakano, and A. Hirose, “Recent advances in physical reservoir computing: A review,” *Neural Networks*, vol. 115, pp. 100 – 123, 2019.
- [15] B. Kia, J. F. Lindner, and W. L. Ditto, “Nonlinear dynamics as an engine of computation,” *Philosophical Transactions of the Royal Society A: Mathematical, Physical and Engineering Sciences*, vol. 375, no. 2088, p. 20160222, 2017.
- [16] A. Clements, J. Fuller, *et al.*, “Forecasting increases in the vix: A time-varying long volatility hedge for equities,” *NCER Working Paper Series 88*, 2012.
- [17] J. Osterrieder, D. Kucharczyk, S. Rudolf, and D. Wittwer, “Neural networks and arbitrage in the vix,” *Digital Finance*, vol. 2, no. 1, pp. 97–115, 2020.
- [18] H. A. *et al.*, “Qiskit: An open-source framework for quantum computing,” 2019.
- [19] C. G. M. CBOE, “CBOE VIX whitepaper,” tech. rep., CBOE, Chicago, Illinois, 2019. accessed Feb 21, 2020.
- [20] C. G. M. CBOE, “The relationship of the SPX and the VIX index,” 2019. Accessed Mar 27, 2020.
- [21] P. Robinson, “A guide to SP500 VIX index,” 2018. Accessed Mar 27, 2020.
- [22] R. S. Hudson and A. Gregoriou, “Calculating and comparing security returns is harder than you think: A comparison between logarithmic and simple returns,” *International Review of Financial Analysis*, vol. 38, pp. 151–162, 2015.
- [23] Anonymous, “Details removed for double blind review,” 2020.
- [24] Anonymous, “Details removed for double blind review,” *NA*, 2020.
- [25] H. Noh, T. You, J. Mun, and B. Han, “Regularizing deep neural networks by noise: Its interpretation and optimization,” in *Advances in Neural Information Processing Systems*, pp. 5109–5118, 2017.

VI. APPENDIX

A. Results for NARMA benchmarking

The Non-linear Auto-regressive Moving Average (NARMA) series is a forecasting task that is commonly employed as a performance benchmark. It has a high degree of non-linearity and dependence on long time lags, leading to significant memory requirements in the forecasting model. We use one step ahead forecasting of the NARMA5 series to benchmark the performance of our quantum reservoir construction. This benchmark was executed using simulated noisy qubits with the noise modeling capabilities available in Qiskit [18]. The NARMA5 series is a temporal sequence defined by:

$$\begin{aligned}
 v_{t+1} &= \alpha v_t + \beta v_t(v_t + v_{t-1} + v_{t-2} + v_{t-3} + v_{t-4}) \\
 &\quad + \gamma s_{t-4} s_t + \delta, \\
 s_t &= \mu \left[\sin \frac{2\pi f_0 t}{T} \sin \frac{2\pi f_1 t}{T} \sin \frac{2\pi f_2 t}{T} + 1 \right].
 \end{aligned} \tag{11}$$

The parameters in Eq. 11 are: $\alpha = 0.30, \beta = 0.05, \gamma = 1.50, \delta = 0.10, \mu = 0.10$, and $f_0 = 2.11, f_1 = 3.73, f_2 = 4.11, T = 100$. These values were originally used in [8] to benchmark quantum reservoirs.

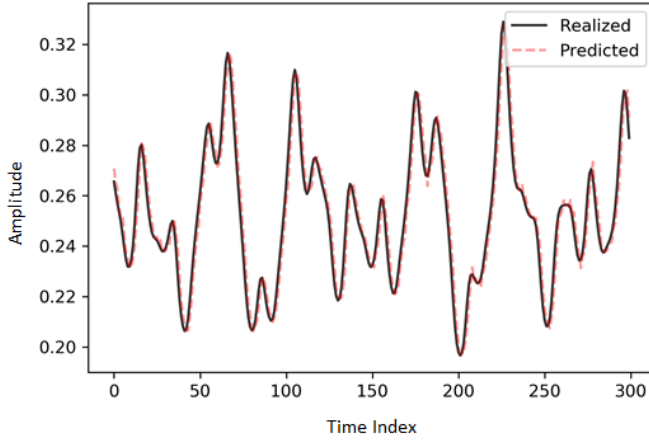


Fig. 17. One-step ahead predictions for the NARMA-5 time-series with the quantum reservoir executed with noisy simulation in Qiskit.

Fig. 17 shows the comparison of realized vs predicted time-series for the NARMA5 task. Only a zoomed-in snapshot is shown of the 5000 point long sequence. The initial one-third of the data was flushed out to allow the system to stabilize. The same optimal configuration that was utilized for VIX forecasting (as discussed in the main text), was also employed here. Our hybrid reservoir achieved an NMSE of 6×10^{-4} . One can compare this to the NMSE obtained in [8] which lied in the range $[3 \times 10^{-3}, 7.6 \times 10^{-6}]$. Thus, the benchmark performance of our hybrid reservoir is comparable to the benchmark performance found in [8]. As in the VIX prediction task, we observe low bias in the prediction error (see Fig. 18).

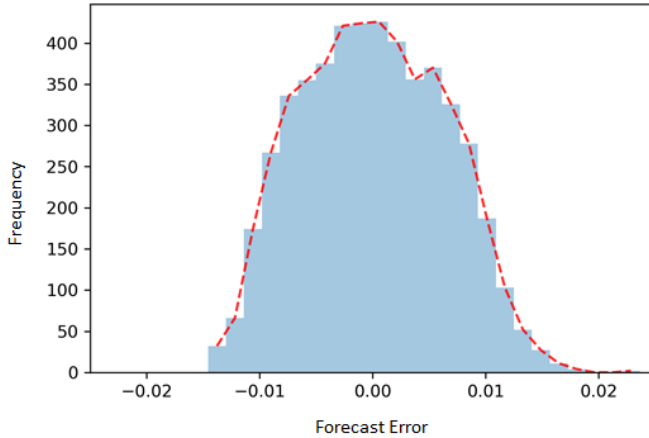


Fig. 18. Histogram of normalized mean square error for the NARMA5 prediction task.

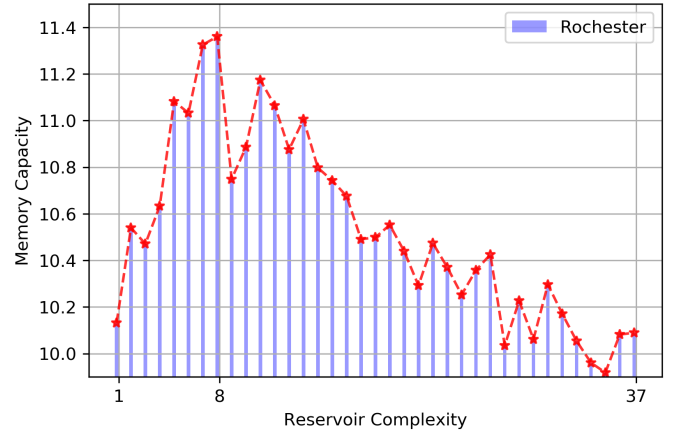


Fig. 19. Variation of Memory Capacity with reservoir complexity for a 8-qubit quantum register on `ibmq_rochester`.

B. Memory capacity of larger reservoirs

In the main text we focused on reservoirs with 6 qubits. We also tested the performance for quantum registers of different sizes. As an example, the memory capacity (MC) characterization described in Section III is repeated for an 8 qubit hybrid reservoir. The sequence of edge densities follow the same sequence as shown in Fig. 2 but for an 8 qubit reservoir there are now 36 graphs. In Fig. 19 we again observe a peak in the MC that occurs for the reservoir with $n - 1 = 7$ self-loops.